Loss Asymmetries in Quantum Traveling-Wave Parametric Amplifiers

M. Houde,[1] L.C.G. Govia,[2,3,*] and A.A. Clerk[2]

[1]*Department of Physics, McGill University, 3600 Rue University, Montréal, Quebec H3A 2T8, Canada*

[2]*Institute for Molecular Engineering, University of Chicago, 5640 S. Ellis Avenue, Chicago, Illinois 60637, USA*

[3]*Raytheon BBN Technologies, 10 Moulton Street, Cambridge, Massachusetts 02138, USA*

We study theoretically how loss impacts the amplification and squeezing performance of a generic quantum traveling-wave parametric amplifier. Unlike previous studies, we analyze how having different levels of loss at signal and idler frequencies can dramatically alter properties compared to the case of frequency-independent loss. We find that loss asymmetries increase the amplifier's added noise in comparison to the symmetric loss case. More surprisingly, even small levels of loss asymmetry can completely destroy any quantum squeezing of symmetric collective-output quadratures, while nonetheless leaving the output state strongly entangled.

I. INTRODUCTION

High-fidelity qubit readout is a crucial ingredient to any viable quantum computing technology. Superconducting qubits operated in circuit QED architectures are among the most promising platforms for quantum computing. Here, readout is typically performed through heterodyne or homodyne detection of the output signal from a cavity dispersively coupled to a qubit [1]. High readout fidelity requires the use of quantum-limited amplifiers [2,3] at the cavity output. The recently developed Josephson traveling-wave parametric amplifier (TWPA), a nondegenerate parametric amplifier built from a chain of Josephson junctions, offers this capability across a broad bandwidth of several GHz [4–6], and will likely be a centerpiece of future circuit QED experiments of increasing size [7,8].

While TWPAs have proven to be excellent signal amplifiers, their utility is not limited to amplification. Even with only vacuum input, the output of an ideal TWPA exhibits broadband two-mode squeezing and entanglement, and can be viewed as a source of two-mode squeezed vacuum states (TMSS). Such states have a myriad of possible applications [9–11]. The collective symmetric quadratures of a TMSS are squeezed below vacuum, which directly enables enhanced readout protocols [12,13]. Further, the signal-idler entanglement generated at the output could be used to entangle remote qubits [14–16], and opens up the possibility for many continuous variable protocols [9], such as quantum teleportation [17].

All of the above applications require high-quality output states, implying that it is necessary to carefully model and understand how loss mechanisms in a TWPA degrade its output; experiments suggest such losses are non-negligible [5]. Previous theoretical studies of loss in TWPAs have either treated the loss as occurring only at the end of the device by introducing a fictitious beam splitter [16], or have considered distributed loss throughout the device, but only for a degenerate amplification regime (where signal and idler are at the same frequency) [18]. Furthermore, these previous treatments consider the case where signal and idler modes of the TWPA have equal (or symmetric) loss rates.

In this work, we extend the methodology of Refs. [16] and [18] to the more general situation of unequal (or asymmetric) signal and idler loss, in both the beam splitter and distributed models of loss (see Fig. 1). Although we are motivated by recent work on Josephson TWPAs, our models and results are general, and thus also apply to more general TWPAs such as those of Refs. [19–22]. Our key results concern the use of TWPAs as squeezing sources. We find that asymmetric loss is detrimental to collective quadrature squeezing: asymmetry feeds amplified noise into the squeezed quadrature, thus quickly suppressing squeezing. This also has implications for applications to continuous variable teleportation [23,24], as well as schemes for enhanced qubit readout [12,13]. We also draw analogy to a cavity-based nondegenerate parametric amplifier (NDPA) source of two-mode squeezing, showing that a similar susceptibility to asymmetry of the internal loss exists for such devices.

We further show how the output states of such models can be understood as thermal two-mode squeezed states. This allows us to quantify the states' entanglement and purity in simple terms. With this description, we find

*luke.c.govia@raytheon.com
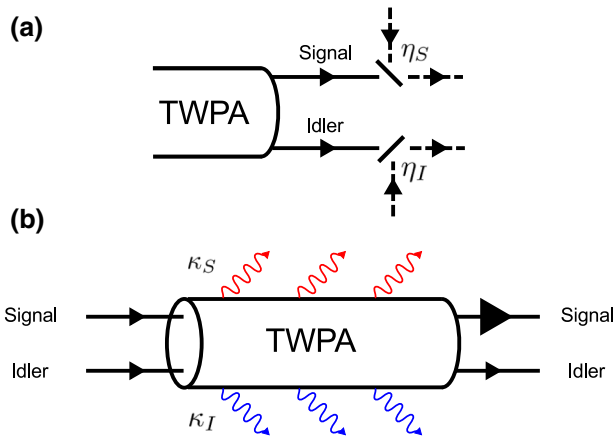
(a)

(b)

FIG. 1.   Schematic figure of two loss models. (a) Beam-splitter loss model: signal and idler modes are passed through beam splitters with transmission coefficients η_S and η_I, respectively. (b) Distributed loss model: signal and idler modes experience different decay rates κ_S and κ_I, respectively, as they propagate through the TWPA.

that these quantities are hardly degraded by asymmetric loss. It is thus possible to have nonzero entanglement while having no squeezing of symmetric collective quadratures below the vacuum level (see Fig. 4). For applications where one requires the symmetric quadratures to be squeezed, we propose a correction protocol to the lossy output state, which allows one to regain squeezing below zero point.

We also analyze the impact of asymmetric loss on the amplification properties of a TWPA. By analyzing the TWPA as a nondegenerate parametric amplifier with distributed loss, we find that asymmetry increases the level of gain (compared to the case of symmetric loss). The amount of noise added by the amplifier is also increased by loss asymmetries; nonetheless, the TWPA still remains nearly quantum limited.

This paper is organized as follows. In Sec. II we outline the generic model of a TWPA, and in Sec. III introduce an ideal way to describe the output of an imperfect TWPA as a thermal two-mode squeezed state. In Sec. IV we consider the effective beam-splitter model of a lossy TWPA, including the effects of asymmetry; we do the same using the distributed model of loss in Sec. V. We quantify the effect of symmetric and asymmetric distributed loss on the output squeezing and gain of the TWPA, thereby characterizing its use as both a squeezing source and an amplifier. Further, we explore the interplay between phase mismatch [4] and asymmetric distributed loss, and compare to a cavity-based NDPA. Our conclusions are finally presented in Sec. VI.

II. MODEL OF AN IDEAL TWPA

As is standard [18], we model a generic TWPA as a nonlinear one-dimensional transmission line or

waveguide. The basic amplification process involves driving the system with a large coherent pump tone (frequency $\bar{\omega}_P$, wavevector $k_P > 0$), which is then scattered by the nonlinearity into photons at signal and idler frequencies. For a four-wave mixing nonlinearity (as is relevant to setups employing Josephson junctions), two pump photons are converted to a pair of signal and idler photons. We consider signal photons with frequency $\omega_S \in (\bar{\omega}_S - D, \bar{\omega}_S + D)$, where D is the maximum bandwidth of interest. Energy conservation then determines the relevant range of idler photons via $\omega_I = 2\bar{\omega}_P - \omega_S$. We focus exclusively on non-degenerate modes of operation, where signal and idler frequencies do not overlap; we thus take $\bar{\omega}_S - D > \bar{\omega}_P$. Given this condition, we can treat signal and idler photons (in the bandwidth of interest) as propagating in effectively independent one-dimensional bosonic channels. We take these fields to have infinite extent, with a nonzero interaction only between positions $x = 0$ and $x = L$. Further, only right-moving signal and idler fields are phase matched to the pump, hence we do not consider left-moving fields (which are decoupled from the dynamics).

To write the system Hamiltonian, we work in a rotating frame at frequency $\bar{\omega}_S$ ($\bar{\omega}_I = 2\bar{\omega}_P - \bar{\omega}_S$) for the signal (idler) channel. Treating the nonlinear interaction at a mean-field level and setting $\hbar = 1$, the basic TWPA Hamiltonian is

$$\hat{H} = \int dx \left\{ \hat{a}_S^\dagger(x) \left(-iv_S \partial_x \right) \hat{a}_S(x) + \hat{a}_I^\dagger(x) \left(-iv_I \partial_x \right) \hat{a}_I(x) \right.$$
$$\left. + \frac{i}{2} \left[\nu(x) \hat{a}_S^\dagger(x) \hat{a}_I^\dagger(x) - \text{H.c.} \right] \right\}. \tag{1}$$

Here, v_n denotes the group velocity of channel $n = S, P, I$, and the lowering operator for channel n is $\hat{b}_n(x) = e^{ik_n x} \hat{a}_n(x)$, where $k_n = \bar{\omega}_n / v_n$. The operators $\hat{a}_n(x)$ describe the spatial envelope of the signal and idler fields, and are canonical bosonic fields: $\left[\hat{a}_n(x), \hat{a}_m^\dagger(x') \right] = \delta(x - x') \delta_{nm}$. Finally, the parametric interaction, with units of a rate, is

$$\nu(x) = \lambda_p(x) e^{-i(k_S + k_I)x} \left[\theta(x) - \theta(x - L) \right], \tag{2}$$

where $\lambda_p(x) = \lambda \psi_P e^{ik_P x}$ for three-wave mixing and $\lambda_p(x) = \lambda |\psi_P|^2 e^{i2k_P x}$ for four-wave mixing, and $\theta(x)$ is the Heaviside function. Here ψ_P is the classical pump amplitude, λ is the bare three- or four-wave mixing interaction strength, and the exponential factor accounts for a lack of phase matching. We start by assuming all group velocities are the same, implying perfect phase matching; $\nu(x)$ can then be taken to be real and positive without any loss of generality.

Working in the Heisenberg picture, the output of our amplifier is described by the operators $\hat{a}_{S/I}(L, t)$, and the input by $\hat{a}_{S/I}(0, t)$. For the ideal TWPA described by Eq. (1), one can easily solve the Heisenberg equations of motion for the system. By relating output fields

to input fields in the frequency domain, one finds the basic scattering relations that characterize the system as a nondegenerate (phase-preserving) amplifier:

$$\hat{a}_S[L,\omega] = e^{i\omega L/v}\sqrt{G_{\text{ideal}}}\,\hat{a}_S[0,\omega]$$
$$+ e^{i\omega L/v}\sqrt{G_{\text{ideal}}-1}\,\hat{a}_I^\dagger[0,\omega], \qquad (3)$$

where we have taken the Fourier transform of our fields, and defined the power gain as

$$G_{\text{ideal}} = \cosh^2(L\nu/v) \equiv \cosh^2(r), \qquad (4)$$

with r denoting the frequency-independent squeezing parameter for our model. Note that in a more realistic model, r is frequency dependent due to, e.g., dispersion effects that cause a lack of phase matching.

In the case where the input fields are just vacuum noise, the output of the ideal TWPA is characterized by the correlation functions

$$\left\langle \hat{a}_{S/I}^\dagger[L,\omega]\hat{a}_{S/I}[L,\omega']\right\rangle = 2\pi\sinh^2(r)\delta[\omega+\omega'], \qquad (5)$$

$$\left\langle \hat{a}_S[L,\omega]\hat{a}_I[L,\omega']\right\rangle = \pi\sinh(2r)\delta[\omega+\omega']. \qquad (6)$$

Note that the frequency-conserving δ functions imply that there are no L-dependent phase factors above. These correlators imply we have perfect two-mode squeezing at each frequency.

Introducing Hermitian quadrature operators via $\hat{a}_{S/I}(L,t) = [\hat{X}_{S/I}(L,t)+i\hat{P}_{S/I}(L,t)]/\sqrt{2}$, we define the symmetric collective quadratures

$$\hat{X}_\pm(L,t) = \frac{\hat{X}_S(L,t)\pm\hat{X}_I(L,t)}{\sqrt{2}}, \qquad (7)$$

with a similar definition for $\hat{P}_\pm(L,t)$. The noise spectral density of a generic quadrature is defined as

$$S_{\hat{X}}[\omega] = \frac{1}{2}\int_{-\infty}^{\infty} dt\, e^{i\omega t}\left\langle\left\{\hat{X}(t),\hat{X}(0)\right\}\right\rangle. \qquad (8)$$

One finds that with the choice of interaction phase in Eq. (1), i.e., $\nu(x)$ taken to be real, the ideal TWPA squeezes fluctuations in both the $\hat{X}_-$ and $\hat{P}_+$ quadratures. The noise spectral density of these squeezed quadratures are

$$S_{\hat{X}_-}^{\text{ideal}}[\omega] = S_{\hat{P}_+}^{\text{ideal}}[\omega] = \frac{1}{2}e^{-2r}. \qquad (9)$$

For any $r > 0$ we obtain squeezing below zero point $(S_{X_-}[\omega] = 1/2)$.

III. THERMAL TWO-MODE SQUEEZED-STATE PARAMETERIZATION OF A LOSSY TWPA

The main goal of this paper is to characterize the output state of an imperfect TWPA. Losses degrade the perfect two-mode squeezing of the signal and idler generated at each frequency by an ideal TWPA. Generically, the state at each frequency is now a thermal two-mode squeezed state (THTMSS). Such a state has the form

$$\hat{\rho}_{\text{THTMSS}} = \hat{S}_2(R)\left[\hat{\rho}_S^{\text{th}}(\bar{n}_S)\otimes\hat{\rho}_I^{\text{th}}(\bar{n}_I)\right]\hat{S}_2^\dagger(R), \qquad (10)$$

where $\hat{S}_2(R) = \exp\left[R\left(\hat{B}_S\hat{B}_I - \text{H.c.}\right)\right]$ is the two-mode squeezing operator for bosonic modes $\hat{B}_{S/I}$ with squeezing parameter R, and $\hat{\rho}_i^{\text{th}}(\bar{n}_i)$ describes a single-mode thermal state with average photon number $\bar{n}_i$. An imperfect TMSS can be fully described by these three parameters: $\bar{n}_S, \bar{n}_I$, and R. In general R can be complex, however, we can always work in a gauge where R is real.

A general THTMSS has the following nonzero correlators:

$$\left\langle\hat{B}_i^\dagger\hat{B}_i\right\rangle = \bar{n}_i + (\bar{n}_S+\bar{n}_I+1)\sinh^2(R), \qquad (11)$$

$$\left\langle\hat{B}_S\hat{B}_I\right\rangle = \frac{\bar{n}_S+\bar{n}_I+1}{2}\sinh(2R), \qquad (12)$$

where $i = S, I$. Note that $\bar{n}_S - \bar{n}_I$ determines the asymmetry of the state (e.g., how different is the state if we exchange the S and I modes). The anomalous entanglement properties of asymmetric THTMSS have been discussed in Ref. [25].

Important properties of the state have a simple expression in terms of the THTMSS description. The purity μ of the state is independent of R and is given by

$$\mu \equiv \text{Tr}\left(\hat{\rho}_{\text{THTMSS}}\right)^2 = \frac{1}{(1+2\bar{n}_S)(1+2\bar{n}_I)}. \qquad (13)$$

The entanglement of the modes S and I in this state can be characterized by the logarithmic negativity [9], and takes the form [26]

$$E_N = -\ln\left[n_R - \sqrt{n_R^2 - (1+2\bar{n}_S)(1+2\bar{n}_I)}\right], \qquad (14)$$

where

$$n_R = (\bar{n}_S+\bar{n}_I+1)\cosh(2R). \qquad (15)$$

Introducing Hermitian quadrature operators via $\hat{B}_{S/I} = (\hat{X}_{S/I}+i\hat{P}_{S/I})/\sqrt{2}$, we define symmetric collective quadratures $\hat{X}_\pm = (\hat{X}_S\pm\hat{X}_I)/\sqrt{2}$. A crucial quantity is the

variance of the squeezed symmetric collective quadrature $\hat{X}_-$,

$$S_{\hat{X}_-} \equiv \langle \hat{X}_-^2 \rangle - \langle \hat{X}_- \rangle^2 = \frac{1}{2}[1 + \bar{n}_S + \bar{n}_I]e^{-2R}. \quad (16)$$

In general, an asymmetric THTMSS ($\bar{n}_S \neq \bar{n}_I$) can be both entangled and have symmetric collective quadrature variances above the vacuum level. We show an example of this in Fig. 2, which plots both the entanglement and symmetric quadrature variance of a THTMSS as a function of $\bar{n}_I$, for constant $\bar{n}_S = 0$ and $R = 1.2$. As can be seen, the variance grows far above vacuum level as $\bar{n}_I$ increases, while the entanglement saturates at a finite value.

Squeezing of the symmetric collective quadrature only goes hand in hand with entanglement in the case of a symmetric THTMSS. For an asymmetric THTMSS, the entanglement is associated with squeezing of an asymmetric collective quadrature, see Sec. IV B 3, and violation of generalized Duan and Tan inequalities [9,27]. Such asymmetric states play a key role in our results, as they describe the output of a TWPA with asymmetric loss.

Finally, note that the multimode output of the TWPA (even with loss) can be understood as a product of THTMSS states. For each frequency ω of interest, we can introduce frequency-resolved temporal modes, defined as

$$\hat{B}_{S/I}^{\text{out}}[\omega] = \lim_{\delta \to 0} \frac{1}{\sqrt{\delta}} \int_{-\delta/2}^{\delta/2} d\omega' \, \hat{a}_{S/I}^{\text{out}}[\pm\omega + \omega'], \quad (17)$$

where the $+$ ($-$) sign is for the signal (idler) mode. These modes have center frequency $\pm\omega$, a vanishing bandwidth δ, and satisfy $\{\hat{B}_j[\omega], \hat{B}_{j'}^\dagger[\omega]\} = \delta_{j,j'}$. For each frequency ω, the pair of modes $\hat{B}_{S/I}^{\text{out}}[\omega]$ is a THTMSS state of the form in Eq. (10), and thus can be completely parameterized by $\bar{n}_S, \bar{n}_I, R$.
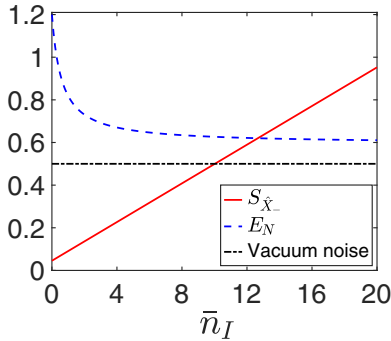

FIG. 2. Symmetric collective quadrature variance (solid red line) and logarithmic negativity (dashed blue line), as a function of $\bar{n}_I$ for an asymmetric THTMSS with $\bar{n}_S = 0$ and $R = 1.2$. The quadrature variance grows beyond vacuum level (dot-dashed black line), indicating amplified noise, even as the entanglement remains finite.

IV. LUMPED-ELEMENT LOSS

We begin our treatment of loss in a TWPA by considering the simplest possible model of loss, the so-called "lumped-element model." Here, we model the final output of a lossy TWPA by applying an independent beam-splitter transformation to each output (S, I) of an ideal TWPA, see Fig. 1(a). The nonunity transmission of the beam splitters corresponds to loss. This model is described by the transformation

$$\hat{a}_S^{\text{out}}[\omega] = \sqrt{\eta_S[\omega]}\hat{a}_S[L, \omega] + \sqrt{1 - \eta_S[\omega]}\hat{\xi}_S[\omega], \quad (18)$$

$$\hat{a}_I^{\text{out}}[\omega] = \sqrt{\eta_I[\omega]}\hat{a}_I[L, \omega] + \sqrt{1 - \eta_I[\omega]}\hat{\xi}_I[\omega], \quad (19)$$

where $\hat{a}_{S/I}[L, \omega]$ are the modes leaving the amplification region of the ideal TWPA, $\eta_{S/I}[\omega]$ are the transmission rates of the signal and idler through the beam splitters, and $\hat{\xi}_{S/I}[\omega]$ are the noise modes coming from the other input ports of the beam splitters. We take this noise to be simple δ-correlated vacuum noise (we consider thermal occupation of these noise modes in Appendix E). Using Eqs. (18) and (19), we find the output-field variances that characterize the output of the lossy TWPA:

$$\left\langle [\hat{a}_S^{\text{out}}[\omega']]^\dagger \hat{a}_S^{\text{out}}[\omega] \right\rangle = 2\pi\eta_S[\omega]\sinh^2(r)\delta[\omega + \omega'], \quad (20)$$

$$\left\langle [\hat{a}_I^{\text{out}}[-\omega']]^\dagger \hat{a}_I^{\text{out}}[-\omega] \right\rangle = 2\pi\eta_I[-\omega]\sinh^2(r)\delta[\omega + \omega'], \quad (21)$$

$$\left\langle \hat{a}_S^{\text{out}}[\omega]\hat{a}_I^{\text{out}}[\omega'] \right\rangle = \pi\sqrt{\eta_S[\omega]\eta_I[\omega']}\sinh(2r)\delta[\omega + \omega']. \quad (22)$$

Recall that the signal and idler channels correspond to different frequency intervals of the single nonlinear transmission line that makes up the TWPA. In the original lab frame, $\eta_S[\omega]$ describes loss at frequency $\bar{\omega}_S + \omega$, whereas $\eta_I[\omega]$ describes loss at frequency $\bar{\omega}_I + \omega = 2\bar{\omega}_P - \bar{\omega}_S + \omega$. It is thus entirely possible that these channels experience different levels of loss. The simplest way to model this is to allow the transmissions $\eta_S[\omega]$ and $\eta_I[\omega]$ to differ from one another. While the effects of symmetric lumped-element loss, $\eta_S = \eta_I$, have been studied previously in Ref. [16], asymmetric loss effects have not.

To quantify the effects of loss asymmetry on the two-mode squeezing between $\hat{a}_S[\omega]$ and $\hat{a}_I[-\omega]$, we use the following parameterization:

$$\eta_S[\omega] = 1 - \bar{\epsilon}(1 + \delta), \quad \eta_I[-\omega] = 1 - \bar{\epsilon}(1 - \delta). \quad (23)$$

Here $\bar{\epsilon}$ describes the average loss and δ is the relative asymmetry; we suppress the explicit ω dependence of ϵ, δ. Without loss of generality we take $\delta > 0$, implying that the signal mode has higher loss than the idler mode. As

discussed in detail below, we find that asymmetry in the loss (i.e., nonzero δ) starts to play a significant role when the average amount of loss is large enough to disrupt the squeezing of an ideal TWPA. This corresponds to the condition $\bar{\epsilon} \gtrsim e^{-2r}$ [cf. Eq. (9)].

A. Thermal two-mode squeezed states

As discussed in Sec. III, for each frequency ω, the output of the lossy TWPA can be mapped onto a thermal TMSS using Eqs. (17) and Eqs. (11), (12). We use this parameterization to discuss the effect of loss.

1. Weak average loss

Consider first the limit of weak average loss, $\bar{\epsilon} \ll 1$ and a large intrinsic squeeze parameter r. Useful expressions are obtained by taking the large-r and small-$\bar{\epsilon}$ limit while keeping $\bar{\epsilon}e^{2r}$ finite and small. This amounts to an expansion in $\bar{\epsilon}e^{2r}$. For purely symmetric loss, $\bar{\epsilon}e^{2r} \ll 1$ implies the amount of vacuum noise added from the loss channels to the output is small enough to not appreciably change the squeezing in the output.

Following this procedure, and expanding the solution to Eqs. (11) and (12) in terms of the small parameter $\bar{\epsilon}$, the effective thermal occupancies $\bar{n}_{S/I}$ are given to second order in $\bar{\epsilon}$ by

$$\bar{n}_{S/I} \approx \frac{1}{4}\left(\bar{\epsilon}e^{2r}\right)(1 \pm \delta) - \frac{1}{16}\left(\bar{\epsilon}e^{2r}\right)^2(1 - \delta^2) + \mathcal{O}(\bar{\epsilon}^3),$$

(24)

where $+/-$ corresponds to S/I. Similarly, the effective squeezing parameter is given by

$$\frac{\cosh(R)}{\cosh(r)} \approx 1 - \frac{1}{4}\left(\bar{\epsilon}e^{2r}\right) + \frac{1}{32}\left(\bar{\epsilon}e^{2r}\right)^2\left(5 - 2\delta^2\right) + \mathcal{O}(\bar{\epsilon}^3).$$

(25)

Thus, in this regime the effect of loss asymmetry is minimal: it only changes the coefficients in the expansions for each parameter, and is not exponentially enhanced (compared to the symmetric loss case). As we now show, this is not true for larger levels of loss.

2. Larger average loss, weak asymmetry

For larger values of average loss, we consider the large-r limit where $\bar{\epsilon}$ is no longer arbitrarily small. In this case, $\bar{\epsilon}e^{2r}$ is no longer a small parameter and we therefore cannot expand with respect to it. Insight is instead obtained by first assuming a weak asymmetry ($\delta \ll 1$) and expanding in δ. We again consider the case of large intrinsic squeezing, and take the asymptotic large-r form of each coefficient in our expansion while keeping $\bar{\epsilon}$ fixed. Doing this, the effective

thermal numbers are given by

$$\bar{n}_{S/I} \approx \frac{\sqrt{(1 - \bar{\epsilon})\bar{\epsilon}}}{2}e^r \pm \frac{e^{2r}}{4}\bar{\epsilon}\delta$$
$$+ \frac{1}{16\sqrt{(1 - \bar{\epsilon})\bar{\epsilon}}}e^{3r}\bar{\epsilon}^2\delta^2 + \mathcal{O}(\delta^3).$$

(26)

We now see that asymmetry has a dramatic effect: for $\delta = 0$ the thermal numbers scale as e^r, whereas with asymmetry (i.e., $\delta \neq 0$), there is a much stronger heating scaling as e^{3r}.

For the effective squeezing parameter in the same weak-δ, large-r regime, we find

$$\frac{\cosh(R)}{\cosh(r)} \approx \frac{\sqrt{1 - \bar{\epsilon}}}{\left[1 + (1 - \bar{\epsilon})\bar{\epsilon}e^{2r}\right]^{1/4}}$$
$$\times \left\{1 - \frac{\bar{\epsilon}^2\delta^2e^{4r}}{16\left[1 + (1 - \bar{\epsilon})\bar{\epsilon}e^{2r}\right]} + \mathcal{O}(\delta^3)\right\}.$$

(27)

Again, we see that the loss-induced suppression of R is more pronounced in the asymmetric loss case.

The above analysis suggests the existence of a kind of crossover: for weak average loss $\bar{\epsilon} < e^{-2r}$, loss asymmetry has a minor effect on our output state, whereas for larger $\bar{\epsilon}$ it has a pronounced effect. This behavior is highlighted in Fig. 3, where we compare the exact behavior of $\bar{n}_{S/I}$ and R as a function of average loss, with and without asymmetry; the crossover scale $\bar{\epsilon} \sim e^{-2r}$ beyond which asymmetry is important is clearly seen.
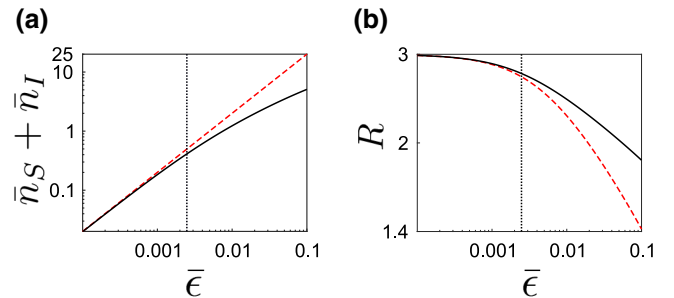

FIG. 3. Properties of the TWPA output state as a function of average loss for the effective beam-splitter model (cf. Sec. IV). Using the THTMSS description, we plot (a) the sum of the average effective thermal photon populations ($\bar{n}_S + \bar{n}_I$) and (b) the effective squeezing parameter R for symmetric (black-solid curve) and fully asymmetric (red-dashed curve, asymmetry parameter $\delta = 1$) loss, as functions of the average loss $\bar{\epsilon}$. The asymmetry parameter is defined in Eq. (23). The vertical dotted lines are markers for the crossover point, $\bar{\epsilon} = e^{-2r}$; for larger $\bar{\epsilon}$ loss asymmetry has a strong impact. The ideal TWPA output squeezing parameter is $r = 3$ for both figures, corresponding to a gain of 20 dB in the loss-free case.

B. Squeezing below vacuum

1. Symmetric loss

Recall that our choice of pump phase ensures that without loss, the collective $\hat{X}_-$ and $\hat{P}_+$ quadratures are squeezed, cf. Eq. (7). For the symmetric loss case ($\eta_S = \eta_I \equiv \eta$), we find directly from Eqs. (20) and (22) that

$$S_{\hat{X}_-}^{\text{sym}}[\omega] = \frac{1}{2}\left[1 - \eta + \eta e^{-2r}\right], \qquad (28)$$

with a similar result for $S_{\hat{P}_+}^{\text{sym}}[\omega]$. As might be expected, with symmetric loss, we simply interpolate between the perfect squeezed state at $\eta = 1$ and a vacuum state when $\eta = 0$. Note that unless the loss level is 100%, there is always some squeezing in the output in this symmetric loss case.

2. Asymmetric loss

When the transmission rates for the signal and idler modes are different, the noise spectral density of the minus quadrature of the output field is

$$S_{\hat{X}_-}^{\text{asym}}[\omega] = \frac{1}{2}\left[\left(1 - \frac{\eta_S + \eta_I}{2}\right) + \frac{e^{-2r}}{4}\left(\sqrt{\eta_S} + \sqrt{\eta_I}\right)^2\right.$$
$$\left. + \frac{e^{2r}}{4}\left(\sqrt{\eta_S} - \sqrt{\eta_I}\right)^2\right]. \qquad (29)$$

In this expression, η_S (η_I) is evaluated at frequency $+\omega$ ($-\omega$). The first bracketed term of Eq. (29) describes the vacuum noise added to the output field as a result of the lossy transmission lines, and the second term describes the usual squeezed noise (which is suppressed when $\eta_s, \eta_I < 1$). The third term, unique to asymmetric loss, describes amplified noise $\propto e^{2r}$ that is now mixed into the minus quadrature due to the asymmetry in the beam splitters' transmission rates. This mixing in of amplified noise is clearly detrimental to achieving squeezing below zero point. In Fig. 4 we see that for larger levels of average loss, the squeezing for asymmetric loss is above zero point, whereas for symmetric loss it is still below zero point. Loss asymmetries can thus have a large impact on the production of squeezing, and greatly affect schemes that use the output of a TWPA as a squeezing source, such as two-mode qubit readout [13] and continuous variable teleportation [17,23,24].

In the context of using a two-mode squeezed state to perform quantum teleportation, Ref. [28] also considered the effect of asymmetric beam-splitter loss. This work derived a similar expression for $S_{\hat{X}_-}^{\text{asym}}[\omega]$, and the results of this paper are consistent with those of Ref. [28].

3. Squeezing of asymmetric collective quadratures

While the symmetric $\hat{X}_-$ collective quadrature rapidly becomes unsqueezed with loss asymmetry, one might ask whether there are other collective quadratures that remain squeezed. It is easy to verify that any symmetric collective quadrature of the form $\sqrt{2}\hat{X}_{\text{sym}} = \hat{X}_S + e^{i\phi}\hat{X}_I$ have a contribution from amplified noise ($\propto e^{2r}$) in its noise spectral density when there is loss asymmetry; hence, loss asymmetry prevents any such quadrature from being squeezed.

That being said, one can define *asymmetric* collective quadratures (i.e., S and I modes weighted unequally) that exhibits squeezing even with asymmetric loss. We define

$$\hat{X}_-^{\text{asym}} = \cos\theta \hat{X}_S^{\text{out}} - \sin\theta \hat{X}_I^{\text{out}}, \qquad (30)$$

$$\hat{P}_+^{\text{asym}} = \cos\theta \hat{P}_S^{\text{out}} + \sin\theta \hat{P}_I^{\text{out}}. \qquad (31)$$

By taking the parameter $\tan\theta = \sqrt{\eta_S/\eta_I}$, one finds

$$S_{\hat{X}_-^{\text{asym}}}[\omega] = \frac{1}{2}\left[1 - \frac{2\eta_S\eta_I}{\eta_S + \eta_I}\left(1 - e^{-2r}\right)\right], \qquad (32)$$

with a similar result for $S_{\hat{P}_+^{\text{asym}}}$; again, in this expression η_S (η_I) are evaluated at frequency $+\omega$ ($-\omega$). We thus see that these quadratures are squeezed below vacuum whenever $r > 0$, irrespective of loss asymmetries. Note crucially that the definition of this quadrature depends sensitively on the amount of loss asymmetry; further for $\theta \neq \pi/4$, the squeezed collective quadratures $\hat{X}_-^{\text{asym}}, \hat{P}_+^{\text{asym}}$ do not commute with one another.

The utility of having such noncommuting, asymmetric quadratures squeezed is mixed. They do imply the
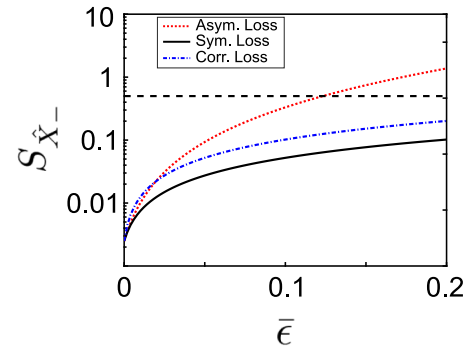

FIG. 4. Output squeezing of the output state of a TWPA, for the beam-splitter model (cf. Sec. IV), as a function of average loss $\bar{\epsilon}$. The squeezing parameter $r = 2.65$, corresponding to a gain of approximately 17 dB. For a fully asymmetric situation where only the signal mode is lossy [i.e., $\delta = 1$ in Eq. (23), red curve], loss can destroy any squeezing below the vacuum level. In contrast, if the loss is symmetric, one always has squeezing below vacuum (black curve). Even with fully asymmetric loss, one can use our proposed correction scheme (cf. Sec. IV D) to regain squeezing below zero point (blue curve). Note that while asymmetric loss can kill vacuum squeezing, signal-idler entanglement always remains nonzero (see Fig. 5).
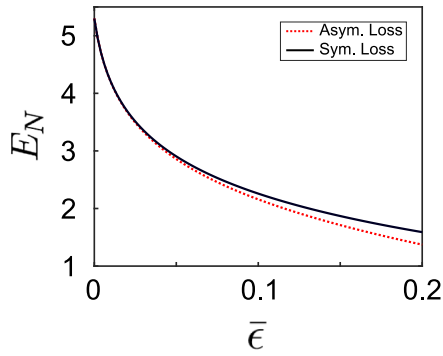
FIG. 5. Logarithmic negativity of the output state of a TWPA, for the beam-splitter model (cf. Sec. IV), as a function of average loss $\bar{\epsilon}$. The squeezing parameter $r = 2.65$, corresponding to a gain of approximately 17 dB. For asymmetric loss (red curve), we consider the maximally asymmetric case where all loss is in the signal mode [i.e., $\delta = 1$ in Eq. (23)]. Logarithmic negativity is much less sensitive to asymmetry (cf. Sec. IV C). Even with asymmetry we retain nonzero logarithmic negativity.

presence of entanglement, as they allow violation of generalized versions of the well-known Duan and Tan inequalities [9,27]. As we see in Sec. IV C, this implies that loss asymmetry does not prevent using the TWPA output state to entangle other systems. However, there are other applications that crucially require two commuting joint quadratures to be squeezed, e.g., the enhanced dispersive measurement scheme described in Ref. [13].

C. Purity and logarithmic negativity

We now study how loss (modeled using the lumped-element approach) impacts the purity and entanglement (as measured by the logarithmic negativity [9]) of the TWPA output state at a given frequency.

1. Symmetric loss

Without any loss asymmetry [i.e., $\delta = 0$ in Eq. (23)], the log negativity is given by

$$E_N = -\ln\left[e^{-2r} + (1 - e^{-2r})\bar{\epsilon}\right]. \tag{33}$$

This saturates to $E_N = \ln[1/\bar{\epsilon}] > 0$ in the large r limit. The logarithmic negativity mimics the behavior of the symmetric squeezed quadrature [see Eq. (28)]: it decreases monotonically from $2r$ to 0 as the loss $\bar{\epsilon}$ increases.

In contrast, the purity of the state for symmetric losses is given by

$$\mu = \frac{1}{1 + 2(1 - \bar{\epsilon})\bar{\epsilon}[\cosh(2r) - 1]}. \tag{34}$$

For any nonzero loss $\bar{\epsilon}$, the purity decays exponentially as e^{-2r} in the large-r limit. Thus, for large intrinsic squeezing r, even a small amount of loss leads to a highly

impure output state that nonetheless possesses a potentially large logarithmic negativity. The utility of such a state in potential applications is thus at first glance somewhat suspect.

To test the utility of such an entangled thermal two-mode squeezed state, we consider the remote entanglement protocol of Ref. [14]. Here, the signal and idler of a TMSS are each sent to a separate qubit, with the goal of stabilizing a two-qubit entangled state (see Appendix A for further details). In the ideal (zero-loss) case, when the signal (idler) qubit is resonant with the signal (idler) mode, the steady state of the two-qubit system is a pure entangled state, and reaches a maximally entangled Bell state in the large gain limit [14].

The situation changes when there is loss, and the output state from the TWPA becomes a THTMSS. Consider first the case where the loss is identical for signal and idler modes, and completely frequency independent. As shown in Ref. [16], the qubit entanglement (quantified by the concurrence [29]) has a distinct maximum as a function of ideal squeezing parameter r (see Fig. 6), which is at odds with the fact that the logarithmic negativity of a THTMSS increases monotonically with r. We show here that this can be simply understood as being a result of the decreasing purity of the THTMSS with increasing r.
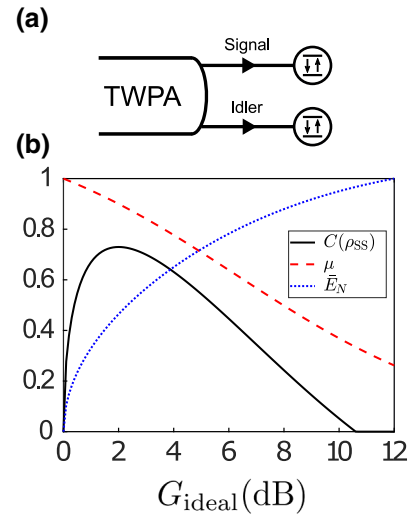

FIG. 6. Signal and idler modes at the output of a TWPA are each sent to separate qubits, resulting in the entanglement of qubits. (a) Schematic figure of protocol. (b) Concurrence [$C(\rho_{SS})$] of the two-qubit steady state of Eq. (A1), along with the purity (μ), and logarithmic negativity (E_N) of the qubits' thermal TMSS environment, all as functions of r. The logarithmic negativity is normalized such that its maximum value is 1, i.e., the plot shows $\bar{E}_N = E_N/E_N^{\max}$. While E_N saturates at a nonzero value, the qubit concurrence has a distinct maximum, eventually dropping to zero as the purity of the thermal TMSS decays. $\bar{\epsilon} = 0.05$ and $\delta = 0$ for these curves.

An example of this is shown in Fig. 6, where we plot the qubit concurrence in the steady state, $C(\rho_{SS})$, as a function of the intrinsic gain $G_{ideal} = \cosh^2 r$ of the TWPA. We also plot the corresponding THTMSS purity and logarithmic negativity (normalized so that its maximum is 1). The qubit concurrence is calculated by solving for the steady state of the master equation given in Appendix A. As can be seen, for increasing r the qubit entanglement initially grows as the THTMSS entanglement; however, very quickly the THTMSS becomes too impure, and the qubit entanglement rapidly decays.

This qubit-based example highlights the fact that the logarithmic negativity alone is not enough to quantify the usefulness of the entanglement found in a THTMSS, and therefore from the output of a lossy TWPA. The purity of the state also plays a crucial role.

2. Asymmetric loss

Extending to the asymmetric case, $\delta \neq 0$, we use the small $\bar{\epsilon}$ expansion for the three THTMSS parameters derived in Sec. III to calculate asymptotic forms of the logarithmic negativity and purity. To second order in $\bar{\epsilon}$ this gives a logarithmic negativity

$$E_N \approx -\ln\left[e^{-2r} + (1 - e^{-2r})\bar{\epsilon} + \tanh(r)\bar{\epsilon}^2\delta^2\right]. \quad (35)$$

While introducing asymmetry further decreases the logarithmic negativity, in the large-r limit asymmetry adds only a constant correction of order $\bar{\epsilon}^2$ to the expression, and hence does not affect the THTMSS entanglement significantly.

The purity, similarly to the logarithmic negativity, is also only minimally affected by asymmetry. In the large-r limit, the expansion takes the form

$$\mu \approx \frac{1}{1 + 2(1 - \bar{\epsilon})\bar{\epsilon}[\cosh(2r) - 1]} - \left[\frac{\bar{\epsilon}\delta}{2(1 - \bar{\epsilon})\bar{\epsilon}}\right]^2 e^{-2r}. \quad (36)$$

As before, the asymmetric correction can be thought of as a renormalization of the coefficient of the exponential decay [since the first term also decays as $\exp(-2r)$ in the large-r limit when $\bar{\epsilon} > 0$].

As neither the logarithmic negativity or purity are affected drastically by loss asymmetry it is likely that an asymmetric version of the two-qubit entanglement protocol considered previously will also be only minimally affected. The concurrence of the two-qubit steady state is shown in Fig. 7 for various amounts of loss asymmetry, and as can be seen, the fully asymmetric case is only marginally worse than the symmetric case. Thus the asymmetric state is almost as useful as the symmetric state for generating two-qubit entanglement.
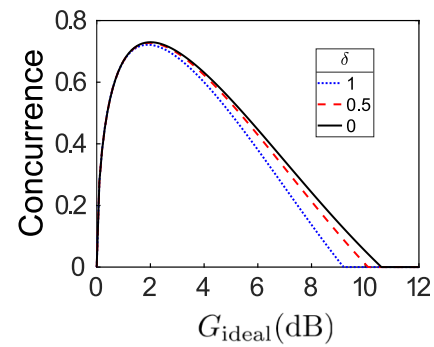

FIG. 7. Concurrence $[C(\rho_{SS})]$ of the two-qubit steady state of Eq. (A1), as a function of r, for various values of loss asymmetry δ, with $\bar{\epsilon} = 0.05$ for all three curves. While an asymmetric THTMSS leads to lower qubit entanglement the difference is minimal, and the asymmetric states perform almost equally as well as the symmetric state in producing qubit entanglement.

D. Correcting for asymmetric loss

We now consider how to correct for asymmetric loss such that we are able to achieve squeezing below vacuum of *symmetric* and commuting joint quadratures, while ideally minimally affecting the purity and logarithmic negativity. The idea here is simple: to counteract asymmetric loss, simply add extra loss to the less lossy channel (i.e., the mode with the larger transmission rate in its effective beam splitter). Recall that without loss of generality we take $\eta_S < \eta_I$ [see Eq. (23)], implying the signal mode has more loss than the idler. Our correction thus corresponds to adding an additional beam splitter at the idler port with transmission rate $\eta_I' < 1$ (thus further attenuating the idler output). Choosing $\eta_I' = \eta_S/\eta_I$ results in a noise spectral density of the final output X_- quadrature given by

$$S_{\hat{X}_-}^{cor} = \frac{1}{2}\left[1 - \eta_S + \eta_S e^{-2r}\right], \quad (37)$$

which for $r > 0$ is below zero point for any $\eta_S > 0$. Remarkably, by deliberately attenuating the output of the lossy TWPA by a specific amount, we regain the possibility of squeezing below zero point in a symmetric joint quadrature, as shown in Fig. 4. Thus, the Tan and Duan inequalities can now be violated while using symmetric, commuting joint quadratures. Further, the purity and logarithmic negativity of the final output state are minimally affected, taking the value of that for symmetric loss with transmission rate η_S. Overall, this deliberate introduction of loss can increase the usefulness of the lumped-element-model lossy TWPA output state in certain applications that require two-mode squeezing of commuting joint quadratures.

V. DISTRIBUTED LOSS

In the beam-splitter model of loss, all losses occur at the end of the amplification region. We now consider a more realistic model of an imperfect TWPA, where loss occurs continuously as photons propagate through the device, and where there is imperfect phase matching between pump, signal, and idler. We start again with the setup shown in Fig. 1(b), as described by Eq. (1). We now allow both signal and idler modes to decay, at independent rates, as they interact parametrically in the region between $x = 0$ to $x = L$.

To implement this distributed loss, we follow the approach used in Ref. [18] to model loss in a degenerate TWPA. We imagine connecting independent loss ports at a set of regularly spaced points x_j along the TWPA; at each point, there is an independent loss channel for signal and for idler photons. These loss ports both provide a means for photons to leave the TWPA, and also inject additional vacuum noise into signal and idler modes (we consider thermal occupation of these noise modes in Appendix E); their effects are described by standard input-output theory. We label the injected vacuum noise from these ports as $\hat{a}_{S/I}^{(\text{loss})}(x)$ (where x labels the noise injected at position x). The coupling rate to the loss port at each point is taken to be the same: κ_S for signal photons, κ_I for idler photons. Finally, we consider the limit where the spacing between the coupling points x_j tends to zero, resulting in a continuous loss per unit length [18].

In addition to this distributed loss, we also now include the effects of imperfect phase matching between pump, signal, and idler modes. Such phase matching is known to be important in realistic TWPAs constructed using Josephson junctions (cf. Refs. [4] and [5]). In such a system, the group velocity is the same for all modes (as they correspond to the same transmission line), but a phase mismatch can arise from nonlinearity-induced frequency shifts. Imperfect phase matching is characterized by a nonzero wavevector mismatch $\Delta k = 2k_P - k_S - k_I$. For nonzero mismatch, the effective parametric drive in the Hamiltonian has a position-dependent phase, cf. Eq. (2), which serves to disrupt amplification.

With both of these imperfections included, the Heisenberg-Langevin equations for our system become

$$\left(\partial_t + v\partial_x + \frac{i\Delta k}{2}\right)\hat{a}_S(x) = \nu\hat{a}_I^\dagger(x) - \frac{\kappa_S}{2}\hat{a}_S(x)$$
$$+ \sqrt{\kappa_S}\hat{a}_S^{(\text{loss})}(x), \quad (38)$$

$$\left(\partial_t + v\partial_x - \frac{i\Delta k}{2}\right)\hat{a}_I^\dagger(x) = \nu\hat{a}_S(x) - \frac{\kappa_I}{2}\hat{a}_I^\dagger(x)$$
$$+ \sqrt{\kappa_I}\hat{a}_I^{\dagger(\text{loss})}(x). \quad (39)$$

Here v is the group velocity (taken to be the same for signal and idler), ν is the parametric interaction strength, and $\kappa_{S/I}$ are the respective decay rates for the signal and idler modes. These equations are valid from $x = 0$ to $x = L$.

Solving the equations of motion in frequency space (see Appendix B), we are able to relate the modes at the end of the amplification regions to those at the beginning, allowing us to calculate the system's scattering matrix and performance as a nondegenerate parametric amplifier. Note that within the approximations we use here, the gain and output squeezing of the TWPA are completely independent of frequency; see Appendix B for more details.

A. Gain

1. Effects of asymmetric loss

For the case of symmetric, distributed loss (i.e., $\kappa_S = \kappa_I$), we find the gain is frequency independent and given by

$$G_{\text{sym}} = e^{-\bar{\kappa}L/v} \cosh^2(L\nu/v)$$
$$\approx \frac{e^{(2\nu-\bar{\kappa})L/v}}{4}, \quad (40)$$

which is equivalent to the result of Ref. [18] obtained for a degenerate parametric amplifier. This result can be mapped to the effective beam-splitter model of loss in Sec. IV, if we take the beam-splitter transmission to be $\eta = e^{-\bar{\kappa}L/v}$.

For the case of asymmetric loss, a simple mapping to the effective beam-splitter model is no longer possible. Letting $\kappa_S = \bar{\kappa} + \epsilon$, $\kappa_I = \bar{\kappa} - \epsilon$, and considering the large length limit, we find the gain with asymmetric loss to be

$$G_{\text{asym}} \approx \frac{e^{(2\tilde{\nu}-\bar{\kappa})L/v}}{4}\left[1 - \frac{\epsilon}{2\tilde{\nu}}\right]^2, \quad (41)$$

where

$$\tilde{\nu} = \sqrt{\nu^2 + \left(\frac{\epsilon}{2}\right)^2}, \quad (42)$$

plays the role of a renormalized interaction amplitude. Comparing symmetric and asymmetric loss results, we see that for fixed average loss $\bar{\kappa}$, introducing loss asymmetry can increase the gain through its exponential dependence on length (outweighing any reduction due to the nonexponential prefactor).

While this might seem surprising, a similar effect occurs in a simple cavity-based nondegenerate parametric amplifier. Following the results of Ref. [3], the zero-frequency gain for such a system is given by

$$\sqrt{G^{\text{cav}}} = \frac{Q^2 + 1}{Q^2 - 1} \quad Q = \frac{2\nu}{\sqrt{\kappa_S\kappa_I}} = \frac{2\nu}{\bar{\kappa}\sqrt{1 - \epsilon^2}}, \quad (43)$$

where $\kappa_{S/I} = \bar{\kappa} \pm \epsilon$ are the coupling rates of signal and idler cavities input-output waveguide, and ν is again the

parametric interaction amplitude. Again, keeping $\bar{\kappa}$ fixed and increasing ϵ increases the gain.

This setup is quite different from a TWPA with distributed loss, as here $\kappa_{S/I}$ represent coupling rates to the input-output ports rather than internal loss rates, and yet a similar effect is observed for the gain in both situations. In Appendix D we consider a cavity-based amplifier with asymmetric internal loss, which is a closer comparison to a TWPA with asymmetric distributed loss.

2. Phase mismatch

We now consider the effects of having imperfect phase matching ($\Delta k \neq 0$) in addition to asymmetric, distributed loss. For small asymmetry and in the large length limit, the gain becomes

$$G \approx e^{-\bar{\kappa}L/v}e^{2L\Re(\tilde{v})/v}\left|1 - \frac{\epsilon + i\Delta k}{2\tilde{v}}\right|^2, \qquad (44)$$

where the effective complex parametric interaction amplitude is defined as

$$\tilde{v} = \sqrt{v^2 + \left(\frac{\epsilon + i\Delta k}{2}\right)^2}. \qquad (45)$$

Without asymmetry, and for large enough Δk, the effective interaction amplitude $\tilde{v}$ becomes purely complex and there is no amplification (i.e., G remains smaller than 1) [4,16]. The above result suggests that the effective increase in the parametric interaction amplitude brought on by loss asymmetry can be used to partially offset the decrease in gain due to phase mismatch.

B. Added noise

We also consider the added noise of our amplifier with distributed loss and imperfect phase matching. Recall that even in the ideal case, a nondegenerate parametric amplifier must add half a quantum of noise to the input signal. To calculate the added noise, denoted by S_{added}, we look at the spectral density of the output signal mode, normalize by the gain and subtract off the input singal contribution to obtain

$$2\pi S_{\text{added}}\delta[\omega + \omega'] \equiv \frac{\langle\{a_{S,\text{out}}[\omega'], a_{S,\text{out}}^{\dagger}[\omega]\}\rangle}{2G_{\text{asym}}}$$
$$- \frac{\langle\{a_{S,\text{in}}[\omega'], a_{S,\text{in}}^{\dagger}[\omega]\}\rangle}{2}. \qquad (46)$$

Including both asymmetric loss and phase mismatch, in the large gain, small asymmetry, and small phase mismatch
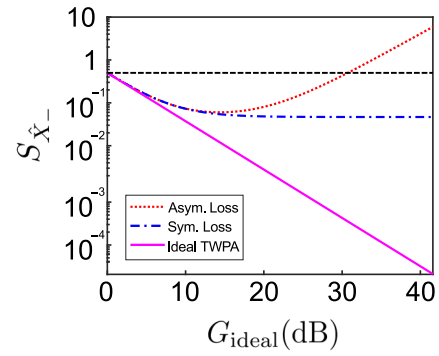

FIG. 8. Output squeezing of a TWPA for the distributed loss model (cf. Sec. V). Curves are plotted as a function of the gain of the ideal distributed model [see Eq. (4)], where the ideal gain is increased by increasing the length L. We set $v/v = 1$, $\bar{\kappa}/v = 1/5$, and $\epsilon = \bar{\kappa}/2$. As we increase gain, asymmetric loss (red curve) goes above zero-point squeezing whereas symmetric loss (blue curve) saturates to a value below zero-point squeezing. The dashed black line represents zero-point squeezing and the pink curve represents the output squeezing of an ideal TWPA.

limit we find that

$$S_{\text{added}} \approx \frac{1}{2} + \frac{1}{2v - \bar{\kappa}}\left[\bar{\kappa} + \epsilon + \frac{(\Delta k^2 - \epsilon^2)}{4v(2v - \kappa)}\right], \qquad (47)$$

independent of frequency. We see that loss increases the added noise above the quantum-limited value of $1/2$, and that this extra noise is sensitive to the amount of asymmetry. The first order in asymmetry term ($\propto \epsilon$) reflects the fact that $\bar{\kappa} + \epsilon$ is the loss of the signal mode. The additional terms (which involve both the amount of phase mismatch and asymmetry ϵ) reflect the effective modification of the parametric interaction amplitude due to imperfections, cf. Eq. (45).

C. Phase-matched symmetric squeezing

Having analyzed how the gain and added noise are affected by asymmetric loss, we now focus on the squeezing. We begin by considering the symmetric case where the signal and idler modes decay at the same rate (i.e., $\kappa_S = \kappa_I \equiv \bar{\kappa}$) and the modes are phase matched ($\Delta k = 0$). In this case, we find that the noise in the squeezed output quadrature is given by

$$S_{\hat{X}_-}^{\text{sym}}[\omega] = \frac{1}{2(\bar{\kappa} + 2v)}\left(\bar{\kappa} + 2ve^{-2Lv/v}e^{-\bar{\kappa}L/v}\right). \qquad (48)$$

Note there is no mixing in of amplified noise, and that taking the large-length limit is always beneficial, as the squeezing decreases monotonically with L, saturating at a value $\bar{\kappa}/[2(2v + \bar{\kappa})]$ (cf. Fig. 8).

We find that for symmetric amounts of loss in signal and idler modes, the distributed loss model predicts

a less severe degradation of squeezing than the lumped-element model of Sec. IV. To see this, we first re-express Eq. (48) as

$$S_{\hat{X}_-}^{\text{sym}}[\omega] = \frac{1}{2}\left[(1-\eta)\,e^{-2r'} + \eta e^{-2r}\right], \qquad (49)$$

where

$$\eta = \frac{2v}{\bar{\kappa}+2v}e^{-\bar{\kappa}L/v}, \qquad (50)$$

$$e^{-2r'} = \frac{\bar{\kappa}}{\bar{\kappa}+2v\left(1-e^{-\bar{\kappa}L/v}\right)}, \qquad (51)$$

and $r = Lv/v$. This expression is reminiscent of Eq. (28) for the squeezing in the lumped-element model of loss. It is in fact equivalent to a lumped-element loss model where squeezed light (characterized by squeezing parameter $r' > 0$) is injected into the dark port of the effective beam splitter (rather than just vacuum noise). By varying the transmission coefficient (via $\bar{\kappa}$), we are interpolating between two different levels of squeezing rather than one level of squeezing and vacuum (no squeezing). Thus, unlike the symmetric lumped-element model, the symmetric distributed model always has squeezing below zero point.

A heuristic understanding of this effect comes from our model of symmetric distributed loss, where we consider vacuum noise entering throughout the TWPA, (i.e., from $x = 0$ to $x = L$). One might naively expect this to be detrimental; however, these fluctuations are themselves squeezed by the TWPA interaction. In fact, by considering a spatially varying decay rate [$\bar{\kappa} = \bar{\kappa}(x)$], we can show that only the fluctuations entering near the end of the TWPA section matter. For such a decay rate, the noise in the squeezed output quadrature takes the form

$$2S_{\hat{X}_-}^{\text{sym}}[\omega] = e^{-(1/v)\int_0^L dx\bar{\kappa}(x)}e^{-2Lv/v}$$
$$+ \frac{1}{v}\int_0^L dx\bar{\kappa}(x)e^{-(1/v)\int_x^L dx'\bar{\kappa}(x')}e^{-2v(L-x)/v}, \qquad (52)$$

where the second term corresponds to the contribution from vacuum fluctuations injected from the loss ports. In the large-length limit and assuming $v \gg \bar{\kappa}(x)\ \forall\ x$, the contribution to the squeezing from the added-noise integral is exponentially insensitive to noise close to the input port. In other words, it is only the added noise coming from a small region near the end of the amplification region that affects the squeezing. Hence, by minimizing the decay rate near the end of the TWPA section, one could obtain higher amounts of squeezing.

This model of a spatially varying decay rate can also be used to treat weak backscattering of the right-moving signal and idler fields into the left-moving fields. This

assumes the left-moving fields are extremely lossy, which prevents multiple scattering events back and forth between the right- and left-moving fields. A full treatment of backscattering and disorder is beyond the scope of this work.

D. Phase-matched asymmetric squeezing

Next, we consider the asymmetric loss case where $\kappa_S \neq \kappa_I$, while keeping the phase-matching condition ($\Delta k = 0$). Without loss of generality, we assume $\kappa_S > \kappa_I$ and define $\kappa_S = \bar{\kappa} + \epsilon$, $\kappa_I = \bar{\kappa} - \epsilon$, where $\bar{\kappa}$ is the average loss and ϵ is the asymmetry. The full expression for $S_{\hat{X}_-}^{\text{asym}}[\omega]$ is cumbersome, and so we consider the low-asymmetry limit. Expanding in the small parameter ϵ/v and keeping only the lowest order term for each possible component of the noise (constant, squeezed, and amplified), we find

$$S_{\hat{X}_-}^{\text{asym}}[\omega] \approx \frac{1}{2(\bar{\kappa}+2v)}\left[\bar{\kappa} + 2ve^{-2L\tilde{v}/v}e^{-\bar{\kappa}L/v}\right]$$
$$+ G_{\text{eff}}\frac{\epsilon^2 e^{-\bar{\kappa}L/v}}{4v(2v-\bar{\kappa})}, \qquad (53)$$

where

$$G_{\text{eff}} = \frac{e^{2L\tilde{v}/v}}{4}, \qquad (54)$$

is an effective gain parameter and $\tilde{v}$ is the renormalized interaction strength given by Eq. (42). As can be seen in Eq. (53), asymmetric distributed loss introduces a component to the noise spectral density, which scales like the gain of the TWPA. Similarly to the result of Eq. (29) for the lumped-element model of asymmetric loss, we find that asymmetric distributed loss introduces amplified noise to the X_- quadrature.

If the gain is large enough this amplified component dominates the noise, even for small asymmetries. This can be seen in Fig. 8. The squeezing for asymmetric distributed loss (red curve) initially goes below zero point, however, as the gain for the ideal TWPA increases, our X^{out} quadrature itself experiences gain. Unlike the symmetric distributed-loss case, there is now an optimal length for maximal squeezing below zero point. Working in the low-asymmetry regime, we find that the optimal length is

$$L_{\text{opt}} \approx \frac{v}{2v}\log\frac{v}{|\kappa_S - \kappa_I|}. \qquad (55)$$

Fortunately, we can do better than just using the optimal length to achieve squeezing below zero point in the asymmetric distributed-loss case. By correcting for the asymmetry, we can remove this length limitation.

However, before addressing how to correct for asymmetry, we again draw analogy with the simple cavity-based

NDPA with asymmetric couplings to the input-output. We find the squeezing given by

$$S_{\hat{X}_-}^{\text{cav}} = \frac{1}{2}\left(\frac{Q-1}{Q+1}\right)^2.$$ (56)

with Q, as defined in Eq. (43), monotonically increasing as a function of the asymmetry. This shows that $S_{\hat{X}_-}^{\text{cav}} \leq 1$ even for large asymmetry, unlike for distributed asymmetric loss in a TWPA where $S_{\hat{X}_-}^{\text{asym}}$ can grow without bound. Thus, in regards to the squeezing, the analogy between the two setups is not as close as it is for the gain.

As described in Appendix D, a closer analog to a TWPA with asymmetric loss is a cavity-based NDPA with symmetric input-output coupling, but asymmetric internal loss. In this case, the squeezing of the symmetric collective quadratures contain a term that is proportional to the gain and the asymmetry (and can grow without bound), similar to what is seen for a TWPA with asymmetric loss. This shows that the results we obtain for the output of an asymmetric TWPA are more generally a property of two-mode squeezed vacuum that experiences asymmetric loss, either during the internal evolution that creates it (distributed-loss TWPA, cavity-based NDPA), or in transmission (lumped-element-loss TWPA).

E. Correcting for asymmetric distributed loss

To correct for the asymmetry, we wish to remove the amplified component of the noise in Eq. (53). In analogy with the lumped-element model, we do so by introducing a beam splitter on the mode with the smaller decay rate (idler mode), therefore adding additional loss to this mode. Using the full expression for $S_{\hat{X}_-}^{\text{asym}}[\omega]$, we find that setting the transmission of this beam splitter to

$$\sqrt{\eta_I} = \frac{\nu}{\sqrt{\nu^2 + \left(\frac{\epsilon}{2}\right)^2} + \frac{\epsilon}{2}},$$ (57)

completely cancels the coefficient of the amplified component of the noise to all orders. The noise is now given, to lowest order, by the expression

$$S_{\hat{X}_-}[\omega] \approx \frac{1}{2(\bar{\kappa}+2\nu)}\left(\bar{\kappa} + 2\nu e^{-2L\tilde{\nu}/v}e^{-\bar{\kappa}L/v}\right)$$
$$+ \frac{1}{4}(1-\eta_I).$$ (58)

We see that the corrected low-asymmetry distributed-loss squeezing is what would be obtained with symmetric distributed loss (at decay rate $\bar{\kappa}$) plus a constant term coming from the additional beam-splitter loss. Once again, the large-length limit is always beneficial after this correction. Importantly, for sufficiently large gain, adding loss

(through the additional beam splitter) allows for squeezing below zero point of the commuting, symmetrically defined collective quadratures X_- and P_+.

VI. CONCLUSION

In this work, we study the effects of frequency-dependent loss on the output state of a TWPA, where photons at signal and idler frequencies see different amounts of dissipation. Within a simple lumped-element model of loss, we show that asymmetric loss can be very detrimental to output squeezing, yet have only minimal effect on the entanglement. It is thus possible to have no joint quadrature squeezing while still having entanglement, and this entanglement may even be useful. By further adding loss to the least lossy mode, we show that we are able to regain squeezing below zero point; this could be useful in applications that require the squeezing of symmetric and commuting collective quadratures.

Using a more realistic distributed-loss model, we show that asymmetric loss increases the gain of the TWPA. By effectively modifying the interaction strength, the exponential dependence of the gain increases. Asymmetric loss can also offset the effects of phase mismatch, to a certain extent, and allow for gain in a situation where it would not occur otherwise. We show that when asymmetric loss in included, there is an optimal length for the TWPA after which output squeezing starts to deteriorate. By mapping the distributed loss to a lumped-element model, we show that distributed loss can be thought of as lumped-element loss, where we inject squeezed noise rather than vacuum, and that the output squeezing can be corrected in a similar manner as for the true lumped-element model.

We show that a hallmark of asymmetric loss in a TWPA is the existence of an asymmetric collective quadrature (with the signal and idler modes weighted unequally) that is squeezed below vacuum noise. This remains true even when the symmetric collective quadratures all have noise above the vacuum level. Combined with the TWPA output remaining a Gaussian state, this is a reliable way to pinpoint asymmetric loss as the most likely source of imperfection. The noise in an asymmetric collective quadrature can be measured as it is for the symmetric case, via classical postprocessing on a shot-to-shot basis of the measurement results for the signal and idler quadratures.

We note that while we are motivated by the Josephson traveling-wave parametric amplifiers used in circuit QED [5], our results apply universally to traveling-wave non-degenerate parametric amplifiers of any design at any frequency [19–22,30–32]. Furthermore, the lumped-element model applies to any two-mode squeezing source that is injected into lossy waveguides [33–36], and our work represents the first exploration of the effects of asymmetric loss in such systems.

APPENDIX A: MASTER EQUATION FOR TWO QUBITS DRIVEN BY AN IMPERFECT TWPA

The evolution of a pair of qubits sharing a correlated environment, as described in Refs. [14] and [16], can be described by the master equation (for a detailed derivation consult Ref. [16])

$$
\dot{\rho}_q = \sum_{k=1,2} \gamma_k \left\{ (1 + N_k) \, \mathcal{D}[\hat{\sigma}_-^k] + N_k \mathcal{D}[\hat{\sigma}_+^k] \right\} \rho_q
$$
$$
- \sqrt{\gamma_1 \gamma_2} M \left(\hat{\sigma}_+^1 \rho_q \hat{\sigma}_+^2 + \hat{\sigma}_+^2 \rho_q \hat{\sigma}_+^1 \right.
$$
$$
\left. - \left\{ \hat{\sigma}_+^1 \hat{\sigma}_+^2, \rho_q \right\} + \text{H.c.} \right), \qquad \text{(A1)}
$$

where $\mathcal{D}[x]\rho = x\rho x^\dagger - \{x^\dagger x, \rho_q\}/2$ is the usual dissipator, $\hat{\sigma}_\pm^k$ are the raising and lowering operators for qubit k, and γ_k is the coupling rate between qubit k and the environment. The thermal photon population of the environment for each qubit (N_k), defined by $\left\langle \hat{a}_k^\dagger(\omega_k) \hat{a}_k(\omega_k') \right\rangle = 2\pi N_k \delta(\omega_k + \omega_k')$, as well as the two-qubit anomalous bath correlator (M), defined by $\left\langle \hat{a}_1(\omega_1) \hat{a}_2(\omega_2) \right\rangle = 2\pi M \delta(\omega_1 + \omega_2)$, depend on the nature of the environment at the qubit frequencies $\omega_{1/2}$. For the output from a lossy TWPA with signal-idler mode resonant with qubit 1/2 at frequency $\omega/-\omega$, these quantities are given by

$$
N_{1/2} = \bar{n}_{S/I} + (\bar{n}_S + \bar{n}_I + 1) \sinh^2(R) = \eta_{S/I} \sinh^2(r), \tag{A2}
$$

$$
M = \frac{\bar{n}_S + \bar{n}_I + 1}{2} \sinh(2R) = \frac{\sqrt{\eta_S \eta_I}}{2} \sinh(2r), \tag{A3}
$$

where we give the form of N_k and M in terms of both the THTMSS parameterization and the lumped-element lossy beam-splitter model. Recall that $\eta_S(\eta_I)$ is evaluated at frequency $\omega(-\omega)$.

For the results of Sec. IV C shown in Figs. 6 and 7, we solve for the steady state of Eq. (A1) numerically, and calculate the concurrence of this state. We set $\gamma_1 = \gamma_2 = \gamma$ for convenience, and in this case the numerical value of γ has no effect on the form of the steady state.

APPENDIX B: DISTRIBUTTED LOSS SOLUTIONS

In this appendix, we provide details on how to obtain the solutions to the distributed-loss model. From the Hamiltonian of Eq. (1) we obtain the following

Heisenberg-Langevin equations of motion:

$$
\left(\partial_t + v\partial_x + \frac{i\Delta k}{2} \right) \hat{a}_S(x) = v\hat{a}_I^\dagger(x) - \frac{\kappa_S}{2} \hat{a}_S(x)
$$
$$
+ \sqrt{\kappa_S} \hat{a}_S^{(\text{loss})}(x), \qquad \text{(B1)}
$$

$$
\left(\partial_t + v\partial_x - \frac{i\Delta k}{2} \right) \hat{a}_I^\dagger(x) = v\hat{a}_S(x) - \frac{\kappa_I}{2} \hat{a}_I^\dagger(x)
$$
$$
+ \sqrt{\kappa_I} \hat{a}_I^{\dagger(\text{loss})}(x), \qquad \text{(B2)}
$$

where $\hat{a}_{S/I}^{(\text{loss})}(x)$ is vacuum noise injected at position x. To obtain the expressions in this form, we gauge away the phase of the parametric interaction [recall Eq. (2)].

Before tackling the full solution, we begin by solving the differential equations without source terms $[\hat{a}_{S/I}^{(\text{loss})}(x)]$. We Fourier transform to frequency space and express everything in matrix form

$$
\partial_x \begin{pmatrix} \hat{a}_S[x, \omega] \\ \hat{a}_I^\dagger[x, \omega] \end{pmatrix}
$$
$$
= \frac{1}{v} \begin{pmatrix} i\omega - (\kappa_S + i\Delta k)/2 & v \\ v & i\omega - (\kappa_I - i\Delta k)/2 \end{pmatrix}
$$
$$
\times \begin{pmatrix} \hat{a}_S[x, \omega] \\ \hat{a}_I^\dagger[x, \omega] \end{pmatrix}. \tag{B3}
$$

The eigenvalues of the matrix on the right-hand side are

$$
\lambda_\pm = \frac{1}{v} \left[i\omega - \left(\frac{\kappa_S + \kappa_I}{4} \right) \pm \sqrt{v^2 + \left(\frac{\kappa_S - \kappa_I + 2i\Delta k}{4} \right)^2} \right], \tag{B4}
$$

and the (unnormalized) eigenvectors are

$$
\vec{v}_\pm = \left[\frac{\kappa_I - \kappa_S - 2i\Delta k}{4v} \pm \sqrt{1 + \left(\frac{\kappa_S - \kappa_I + 2i\Delta k}{4v} \right)^2}, 1 \right]^T. \tag{B5}
$$

The solutions are given by

$$
\begin{pmatrix} \hat{a}_S[x, \omega] \\ \hat{a}_I^\dagger[x, \omega] \end{pmatrix} = C_1 e^{\lambda_+ x} \vec{v}_+ + C_2 e^{\lambda_- x} \vec{v}_-. \tag{B6}
$$

We use the boundary conditions $\hat{a}_S[x = 0, \omega] = \hat{a}_S[0, \omega]$ and $\hat{a}_I^\dagger[x = 0, \omega] = \hat{a}_I^\dagger[0, \omega]$. We know the signal and idler that enters the chain and we wish to study how they evolve along the TWPA. From these boundary conditions, we can obtain expressions for the coefficients C_1 and C_2:

$$C_1 = \frac{\hat{a}_S[0,\omega] - \left[\frac{\kappa_I - \kappa_S - 2i\Delta k}{4v} - \sqrt{1 + \left(\frac{\kappa_S - \kappa_I + 2i\Delta k}{4v} \right)^2} \right] \hat{a}_I^\dagger[0,\omega]}{2\sqrt{1 + \left(\frac{\kappa_S - \kappa_I + 2i\Delta k}{4v} \right)^2}}, \tag{B7}$$

$$C_2 = -\frac{\hat{a}_S[0,\omega] - \left[\frac{\kappa_I - \kappa_S - 2i\Delta k}{4v} + \sqrt{1 + \left(\frac{\kappa_S - \kappa_I + 2i\Delta k}{4v} \right)^2} \right] \hat{a}_I^\dagger[0,\omega]}{2\sqrt{1 + \left(\frac{\kappa_S - \kappa_I + 2i\Delta k}{4v} \right)^2}}. \tag{B8}$$

We now wish to express the solutions in the form of a scattering matrix equation

$$\begin{pmatrix} \hat{a}_S[x,\omega] \\ \hat{a}_I^\dagger[x,\omega] \end{pmatrix} = \begin{pmatrix} s_{\hat{a}_S,\hat{a}_S}[x,\omega] & s_{\hat{a}_S,\hat{a}_I^\dagger}[x,\omega] \\ s_{\hat{a}_I^\dagger,\hat{a}_S}[x,\omega] & s_{\hat{a}_I^\dagger,\hat{a}_I^\dagger}[x,\omega] \end{pmatrix} \begin{pmatrix} \hat{a}_S[0,\omega] \\ \hat{a}_I^\dagger[0,\omega] \end{pmatrix}. \tag{B9}$$

Using the form of C_1 and C_2 above, we isolate in terms of $\hat{a}_S[0,\omega]$ and $\hat{a}_I^\dagger[0,\omega]$. The elements of the scattering matrix are

$$s_{\hat{a}_S,\hat{a}_S}[x,\omega] = e^{[i\omega - (\kappa_S + \kappa_I)/4]x/v} \left[\cosh(x\tilde{v}/v) \right.$$
$$\left. + \frac{\kappa_I - \kappa_S - 2i\Delta k}{4\tilde{v}} \sinh(x\tilde{v}/v) \right],$$

$$s_{\hat{a}_S,\hat{a}_I^\dagger}[x,\omega] = s_{\hat{a}_I^\dagger,\hat{a}_S}[x,\omega] = e^{[i\omega - (\kappa_S + \kappa_I)/4]x/v} \frac{v \sinh(x\tilde{v}/v)}{\tilde{v}},$$

$$s_{\hat{a}_I^\dagger,\hat{a}_I^\dagger}[x,\omega] = e^{[i\omega - (\kappa_S + \kappa_I)/4]x/v} \left[\cosh(x\tilde{v}/v) \right.$$
$$\left. - \frac{\kappa_I - \kappa_S - 2i\Delta k}{4\tilde{v}} \sinh(x\tilde{v}/v) \right], \tag{B10}$$

where

$$\tilde{v} = \sqrt{v^2 + \left(\frac{\kappa_S - \kappa_I + 2i\Delta k}{4} \right)^2}. \tag{B11}$$

We can construct the full solution to the differential equation, including the source terms, using these scattering matrix elements. The full solution is given by

$$\begin{pmatrix} \hat{a}_S[x,\omega] \\ \hat{a}_I^\dagger[x,\omega] \end{pmatrix} = \mathbf{s}[x,\omega] \begin{pmatrix} \hat{a}_S(0) \\ \hat{a}_I^\dagger(0) \end{pmatrix} + \frac{1}{v} \int_0^x dx' \mathbf{s}[\mathbf{x} - \mathbf{x}', \omega]$$
$$\times \begin{pmatrix} \sqrt{\kappa_S} \hat{a}_S^{(\text{loss})}[x',\omega] \\ \sqrt{\kappa_I} \hat{a}_I^{\dagger(\text{loss})}[x',\omega] \end{pmatrix}, \tag{B12}$$

where $\mathbf{s}(\mathbf{x})$ is the transfer matrix defined with the above elements in Eq. (B10).

APPENDIX C: LOGARITHMIC NEGATIVITY AND PURITY

In this section, we derive the form of Eq. (14) from its definition based on the covariance matrix of a two-mode squeezed state (taking our two modes to be the signal and idler modes). We define a four-dimensional basis vector $\hat{\mathbf{X}} = (\hat{X}_S, \hat{P}_S, \hat{X}_I, \hat{P}_I)^\mathrm{T}$. In this basis, the covariance matrix takes the form

$$\sigma = \begin{pmatrix} 2\langle \hat{a}_S^\dagger \hat{a}_S \rangle + 1 & 0 & \langle \hat{a}_I \hat{a}_S \rangle + \langle \hat{a}_I^\dagger \hat{a}_S^\dagger \rangle & 0 \\ 0 & 2\langle \hat{a}_S^\dagger \hat{a}_S \rangle + 1 & 0 & -\langle \hat{a}_I \hat{a}_S \rangle - \langle \hat{a}_I^\dagger \hat{a}_S^\dagger \rangle \\ \langle \hat{a}_I \hat{a}_S \rangle + \langle \hat{a}_I^\dagger \hat{a}_S^\dagger \rangle & 0 & 2\langle \hat{a}_I^\dagger \hat{a}_I \rangle + 1 & 0 \\ 0 & -\langle \hat{a}_I \hat{a}_S \rangle - \langle \hat{a}_I^\dagger \hat{a}_S^\dagger \rangle & 0 & 2\langle \hat{a}_I^\dagger \hat{a}_I \rangle + 1 \end{pmatrix}. \tag{C1}$$

To find the logarithmic negativity, we need to take the partial transpose of the covariance matrix and then find its eigenvalues. The logarithmic negativity is given by

$$E_N = -\sum_i \ln \lambda_i, \qquad (C2)$$

where λ_i are distinct eigenvalues with a value less than 1. Due to its symplectic form, the partially transposed covariance matrix only has two distinct eigenvalues. Of those two, only one will ever be less than 1. We find the eigenvalues to be

$$\lambda_\pm = \langle \hat{a}_S^\dagger \hat{a}_S \rangle + \langle \hat{a}_I^\dagger \hat{a}_I \rangle + 1$$
$$\pm \sqrt{\left(\langle \hat{a}_S^\dagger \hat{a}_S \rangle - \langle \hat{a}_I^\dagger \hat{a}_I \rangle \right)^2 + \left(\langle \hat{a}_I \hat{a}_S \rangle + \langle \hat{a}_I^\dagger \hat{a}_S^\dagger \rangle \right)^2}, \quad (C3)$$

where only λ_- can ever be less than 1.

We can now express the needed averages using the thermal TMSS parameters as introduced in Eqs. (11) and (12). A straightforward calculation then yields

$$E_N = -\ln\left[n_R - \sqrt{n_R^2 - (1 + 2\bar{n}_S)(1 + 2\bar{n}_I)} \right]. \quad (C4)$$

The purity, as a function of the covariance matrix is given by

$$\mu = \frac{1}{\sqrt{\det(\sigma)}}. \qquad (C5)$$

For the case of a TMSS, the eigenvalues of the covariance matrix are the same as the partially transposed one. Since the eigenvalues are repeated, the determinant can be expressed as

$$\det = (\lambda_+)^2 (\lambda_-)^2$$
$$= \left\{ n_R^2 - \left[\sqrt{n_R^2 - (1 + 2\bar{n}_S)(1 + 2\bar{n}_I)} \right]^2 \right\}^2$$
$$= [(1 + 2\bar{n}_S)(1 + 2\bar{n}_I)]^2. \qquad (C6)$$

Hence, the purity takes the form

$$\mu = \frac{1}{(1 + 2\bar{n}_S)(1 + 2\bar{n}_I)}. \qquad (C7)$$

APPENDIX D: CAVITY-BASED NONDEGENERATE PARAMETRIC AMPLIFIER WITH INTERNAL LOSS

Here we consider the effects of having additional internal loss for a cavity-based nondegenerate parametric amplifier. The Heisenberg-Langevin equations for this system are

$$\dot{\hat{a}}_S = v\hat{a}_I^\dagger - \left(\frac{\kappa_S + \gamma_S}{2} \right) \hat{a}_S - \sqrt{\kappa_S}\hat{a}_{S,\text{in}} - \sqrt{\gamma_S}\hat{b}_{S,\text{in}}, \quad (D1)$$

$$\dot{\hat{a}}_I^\dagger = v\hat{a}_S - \left(\frac{\kappa_I + \gamma_I}{2} \right) \hat{a}_I^\dagger - \sqrt{\kappa_I}\hat{a}_{I,\text{in}}^\dagger - \sqrt{\gamma_I}\hat{b}_{I,\text{in}}^\dagger, \quad (D2)$$

where we treat the internal loss as coming from another waveguide with couplings $\gamma_{S/I}$ and noise modes $\hat{b}_{S/I,\text{in}}$. Using the input-output relations, the steady-state solution for the output field of the X_- collective quadrature is given by

$$\sqrt{2}\hat{X}_-^{\text{out}} = \left(1 + \frac{2\kappa_S\sigma_I - 4v\sqrt{\kappa_S\kappa_I}}{4v^2 - \sigma_S\sigma_I} \right) \hat{X}_{S,\text{in}}$$
$$- \left(1 + \frac{2\kappa_I\sigma_S - 4v\sqrt{\kappa_S\kappa_I}}{4v^2 - \sigma_S\sigma_I} \right) \hat{X}_{I,\text{in}}$$
$$+ \left(\frac{2\sqrt{\kappa_S\gamma_S}\sigma_I - 4v\sqrt{\kappa_I\gamma_S}}{4v^2 - \sigma_S\sigma_I} \right) \hat{X}_{S,\text{in}}^b$$
$$- \left(\frac{2\sqrt{\kappa_I\gamma_I}\sigma_S - 4v\sqrt{\kappa_I\gamma_I}}{4v^2 - \sigma_S\sigma_I} \right) \hat{X}_{I,\text{in}}^b, \quad (D3)$$

where $\sigma_{S/I} = \kappa_{S/I} + \gamma_{S/I}$, and the superscript b denotes the additional noise modes.

Focussing on the squeezing in the case that the input-output couplings are equal ($\kappa_S = \kappa_I = \bar{\kappa}$), we consider general asymmetric internal loss, described by $\gamma_{S/I} = \bar{\gamma} \pm \epsilon$. In the situation where both $\bar{\gamma}$ and ϵ are small compared to v and $\bar{\kappa}$, we find to lowest order that

$$S_{\hat{X}_-}[\omega] = \frac{1}{2} \left(\frac{Q-1}{Q+1} \right)^2 + \frac{1}{(Q+1)^3} \frac{8v\bar{\gamma}}{\bar{\kappa}^2}$$
$$+ G^{\text{cav}} \frac{4(3Q-1)}{(Q^2+1)^2(Q+1)} \frac{v\epsilon^2}{\kappa^5}, \quad (D4)$$

where G^{cav} is defined as before, and for symmetric coupling $Q = 2v/\bar{\kappa}$. This shows that there is a correction term that is linear in the average internal loss, $\bar{\gamma}$, and one that is quadratic in the asymmetry, ϵ. As with distributed loss in the TWPA, the asymmetric correction is amplified as it scales with the gain.

APPENDIX E: THERMAL OCCUPATION OF THE NOISE MODES

1. Beam-splitter model

We begin with the beam-splitter model and we allow for the noise modes $\hat{\xi}_{S/I}$ to be thermally occupied such

that $\langle \hat{\xi}_{S/I}^{\dagger} \hat{\xi}_{S/I} \rangle = \bar{m}_{S/I}$. The noise in the squeezed output quadrature is given by

$$S_{\hat{X}_-}^{\text{therm}}[\omega] = S_{\hat{X}_-}^{\text{asym}}[\omega] + \frac{1 - \eta_S}{2} \bar{m}_S + \frac{1 - \eta_I}{2} \bar{m}_I, \quad \text{(E1)}$$

where $S_{\hat{X}_-}^{\text{asym}}$ is the expression of Eq. (29). As can be seen, this is simply a constant correction to that found in the main text. We note that this result agrees with that found in Ref. [28].

2. Distributed-loss model

For the distributed-loss model, we assume the internal loss modes are thermally occupied and that this thermal occupation is constant along the whole length of the TWPA. For symmetric loss, we find that with thermal noise the noise in the squeezed output quadrature is

$$S_{\hat{X}_-}^{\text{therm}}[\omega] = S_{\hat{X}_-}^{\text{sym}}[\omega] + \frac{\kappa \left[1 - e^{-(2\nu + \kappa)L/v} \right]}{2(2\nu + \kappa)} (\bar{m}_S + \bar{m}_I), \quad \text{(E2)}$$

where $S_{\hat{X}_-}^{\text{sym}}[\omega]$ is from Eq. (48). This is once again a constant correction, which increases with increasing length.

For asymmetric distributed loss, we follow the same procedure in the main text and find to lowest order in the asymmetry and average loss that

$$\begin{aligned} S_{\hat{X}_-}^{\text{therm}}[\omega] = {}& S_{\hat{X}_-}^{\text{asym}}[\omega] + \frac{\bar{\kappa} \left[1 - e^{-(2\tilde{\nu} + \bar{\kappa})L/v} \right]}{2(2\nu + \bar{\kappa})} (\bar{m}_S + \bar{m}_I) \\ & + \frac{\epsilon}{4\nu} \left[1 - e^{-(2\tilde{\nu} + \bar{\kappa})L/v} \right] (\bar{m}_S - \bar{m}_I) \\ & + \frac{\bar{\kappa} \epsilon^2}{8\nu^2 (2\nu - \bar{\kappa})} G_{\text{eff}} e^{-\bar{\kappa}L/v} (\bar{m}_S + \bar{m}_I), \quad \text{(E3)} \end{aligned}$$

where $S_{\hat{X}_-}^{\text{asym}}[\omega]$ is from Eq. (53). Asymmetry again feeds additional amplified noise into the squeezed quadrature. However, note the emergence of a linear in ϵ contribution, which comes from the fact that the signal and idler need not have equal thermal populations, and that $\kappa_{S/I} = \bar{\kappa} \pm \epsilon$.

---

[1] A. Blais, R.-S. Huang, A. Wallraff, S. M. Girvin, and R. J. Schoelkopf, Cavity quantum electrodynamics for superconducting electrical circuits: An architecture for quantum computation, Phys. Rev. A **69**, 062320 (2004).

[2] C. M. Caves, Quantum limits on noise in linear amplifiers, Phys. Rev. D **26**, 1817 (1982).

[3] A. A. Clerk, M. H. Devoret, S. M. Girvin, F. Marquardt, and R. J. Schoelkopf, Introduction to quantum noise, measurement, and amplification, Rev. Mod. Phys. **82**, 1155 (2010).

[4] K. O'Brien, C. Macklin, I. Siddiqi, and X. Zhang, Resonant Phase Matching of Josephson Junction Traveling Wave Parametric Amplifiers, Phys. Rev. Lett. **113**, 157001 (2014).

[5] C. Macklin, K. O'Brien, D. Hover, M. E. Schwartz, V. Bolkhovsky, X. Zhang, W. D. Oliver, and I. Siddiqi, A near-quantum-limited Josephson traveling-wave parametric amplifier, Science **350**, 307 (2015).

[6] T. C. White *et al.*, Traveling wave parametric amplifier with josephson junctions using minimal resonator phase matching, Appl. Phys. Lett. **106**, 242601 (2015).

[7] A. G. Fowler, M. Mariantoni, J. M. Martinis, and A. N. Cleland, Surface codes: Towards practical large-scale quantum computation, Phys. Rev. A **86**, 032324 (2012).

[8] R. Versluis, S. Poletto, N. Khammassi, B. Tarasinski, N. Haider, D. J. Michalak, A. Bruno, K. Bertels, and L. DiCarlo, Scalable Quantum Circuit and Control for a Superconducting Surface Code, Phys. Rev. Appl. **8**, 034021 (2017).

[9] S. L. Braunstein and P. van Loock, Quantum information with continuous variables, Rev. Mod. Phys. **77**, 513 (2005).

[10] C. Weedbrook, S. Pirandola, R. García-Patrón, N. J. Cerf, T. C. Ralph, J. H. Shapiro, and S. Lloyd, Gaussian quantum information, Rev. Mod. Phys. **84**, 621 (2012).

[11] A. I. Lvovsky, in *Photonics, Volume 1: Fundamentals of Photonics and Physics*, edited by D. L. Andrews (Wiley, West Sussex, UK, 2015), Chap. 5, p. 121.

[12] S. Barzanjeh, D. P. DiVincenzo, and B. M. Terhal, Dispersive qubit measurement by interferometry with parametric amplifiers, Phys. Rev. B **90**, 134515 (2014).

[13] N. Didier, A. Kamal, W. D. Oliver, A. Blais, and A. A. Clerk, Heisenberg-Limited Qubit Read-Out with Two-Mode Squeezed Light, Phys. Rev. Lett. **115**, 093604 (2015).

[14] B. Kraus and J. I. Cirac, Discrete Entanglement Distribution with Squeezed Light, Phys. Rev. Lett. **92**, 013602 (2004).

[15] N. Didier, J. Guillaud, S. Shankar, and M. Mirrahimi, Remote entanglement stabilization and concentration by quantum reservoir engineering, Phys. Rev. A **98**, 012329 (2018).

[16] A. L. Grimsmo and A. Blais, Squeezing and quantum state engineering with josephson travelling wave amplifiers, npj Quant. Inf. **3**, 20 (2017).

[17] A. Furusawa, J. L. Sørensen, S. L. Braunstein, C. A. Fuchs, H. J. Kimble, and E. S. Polzik, Unconditional quantum teleportation, Science **282**, 706 (1998).

[18] C. M. Caves and D. D. Crouch, Quantum wideband traveling-wave analysis of a degenerate parametric amplifier, J. Opt. Soc. Am. B **4**, 1535 (1987).

[19] B. Ho Eom, P. K. Day, H. G. LeDuc, and J. Zmuidzinas, A wideband, low-noise superconducting amplifier with high dynamic range, Nat. Phys. **8**, 623 (2012).

[20] A. A. Adamyan, S. E. de Graaf, S. E. Kubatkin, and A. V. Danilov, Superconducting microwave parametric amplifier based on a quasi-fractal slow propagation line, J. Appl. Phys. **119**, 083901 (2016).

[21] M. R. Vissers, R. P. Erickson, H.-S. Ku, L. Vale, X. Wu, G. C. Hilton, and D. P. Pappas, Low-noise kinetic inductance traveling-wave amplifier using three-wave mixing, Appl. Phys. Lett. **108**, 012601 (2016).

[22] R. P. Erickson and D. P. Pappas, Theory of multiwave mixing within the superconducting kinetic-inductance traveling-wave amplifier, Phys. Rev. B **95,** 104506 (2017).

[23] G. Adesso and F. Illuminati, Equivalence between Entanglement and the Optimal Fidelity of Continuous Variable Teleportation, Phys. Rev. Lett. **95,** 150503 (2005).

[24] M. S. Kim and J. Lee, Asymmetric quantum channel for quantum teleportation, Phys. Rev. A **64,** 012309 (2001).

[25] G. Adesso, A. Serafini, and F. Illuminati, Extremal entanglement and mixedness in continuous variable systems, Phys. Rev. A **70,** 022318 (2004).

[26] Y.-D. Wang, S. Chesi, and A. A. Clerk, Bipartite and tripartite output entanglement in three-mode optomechanical systems, Phys. Rev. A **91,** 013807 (2015).

[27] S. M. Tan, Confirming entanglement in continuous variable quantum teleportation, Phys. Rev. A **60,** 2752 (1999).

[28] R. Di Candia, K. Fedorov, L. Zhong, S. Felicetti, E. Menzel, M. Sanz, F. Deppe, A. Marx, R. Gross, and E. Solano, Quantum teleportation of propagating quantum microwaves, EPJ Quant. Technol. **2,** 25 (2015).

[29] W. K. Wootters, Entanglement of formation and concurrence, Quant. Inf. Comput. **1,** 27 (2001).

[30] C. Kim and P. Kumar, Quadrature-squeezed Light Detection Using a Self-generated Matched Local Oscillator, Phys. Rev. Lett. **73,** 1605 (1994).

[31] V. Boyer, A. M. Marino, R. C. Pooser, and P. D. Lett, Entangled images from four-wave mixing, Science **321,** 544 (2008).

[32] C. S. Embrey, M. T. Turnbull, P. G. Petrov, and V. Boyer, Observation of Localized Multi-spatial-mode Quadrature Squeezing, Phys. Rev. X **5,** 031004 (2015).

[33] C. Eichler, D. Bozyigit, C. Lang, M. Baur, L. Steffen, J. M. Fink, S. Filipp, and A. Wallraff, Observation of Two-mode Squeezing in the Microwave Frequency Domain, Phys. Rev. Lett. **107,** 113601 (2011).

[34] J. U. Fürst, D. V. Strekalov, D. Elser, A. Aiello, U. L. Andersen, C. Marquardt, and G. Leuchs, Quantum Light from a Whispering-gallery-mode Disk Resonator, Phys. Rev. Lett. **106,** 113901 (2011).

[35] M. Förtsch, J. U. Fürst, C. Wittmann, D. Strekalov, A. Aiello, M. V. Chekhova, C. Silberhorn, G. Leuchs, and C. Marquardt, A versatile source of single photons for quantum information processing, Nat. Comm. **4,** 1818 (2013).

[36] C. Reimer, M. Kues, P. Roztocki, B. Wetzel, F. Grazioso, B. E. Little, S. T. Chu, T. Johnston, Y. Bromberg, L. Caspani, D. J. Moss, and R. Morandotti, Generation of multiphoton entangled quantum states by means of integrated frequency combs, Science **351,** 1176 (2016).